

Adaptive Multiple MPC for a Wind Farm with DFIG: a Decentralized-Coordinated Approach

Xiao-ming LI[†], Xi ZHANG^{*}, Zhong-wei LIN^{**}, Yu-guang NIU^{**}, Ming-yang LI^{**}
and Noel Vishal Nathan^{***}

Abstract – For low investment and flexible control, doubly fed induction generator (DFIG) is becoming the dominant type that is been used in the wind farms (WFs) today. The report researches about the rotor-side controller of DFIG where all design is based on the single machine infinite bus (SMIB) model. The interactions between the different generators have not been considered in the SMIB model, and the desired performance cannot be obtained by using the controller based on this model. In this situation, an adaptive decentralized-coordinated multiple model predictive control (ADM-MPC) is proposed. First, the interaction measurement method is developed to obtain the interaction measurement model of DFIG, where the interactions between the different generators have been considered. Next, an adaptive multiple MPC based on the obtained interaction measurement method of DFIG is employed to control the rotor-side converter of DFIG. In order to cope with the stochastic disturbance of wind turbine, the augment state structure is employed to improve the tracking control performance. An artificial neural network (ANN) trained online is employed as a weighting controller to cope with the nonlinearities and large operating range of DFIG. A simple, generic renewable power system (RPS) is used to demonstrate contributions. The results of both dominant eigenvalue analysis and time response simulations are represented to illustrate contributions to system damping and transient stability that the DFIG based WF can make with the proposed ADM-MPC controller.

Keywords: Doubly fed induction generator, Decentralized-coordinated control, Interaction measurement method, Transient stability, System damping

1. Introduction

During the last decade, wind energy has shown the world's fastest rate of growth of any form of electric power generations [1] and many wind power generators have been integrated into power systems, which causes the share of wind power to reach a considerable level [2]. It has been demonstrated that the continuing integration of new large WFs into the power systems can influence the stabilities of power systems [3, 4].

Because of low investment and flexible control, DFIG is becoming the most popular type used in the grid connected WFs [5]. The design of DFIG control system is not a straight forward task. One of the main reasons is that the DFIG is a multiple-input-multiple-output system with strongly-coupled variables. Furthermore, the system nonlinearity and the stochastic variation of input

mechanism torque make the control design method more difficult.

A conventional proportion integration differentiation (PID) controller based decoupling control strategy for the active power and reactive power proposed in [6] has been widely used in control of DFIG [7-9]. For reliability and simplicity, the conventional PID controllers are well accepted in the engineering field, and those have been widely used in power systems. However, the parameters of the conventional PID controllers are usually tuned with the approximated linearized model. In this situation, there must be a compromise between the control performance and robustness.

The control of DFIG using MPC method has been the subject of many recent contexts [10-15], which are all based on SMIB model. The SMIB model ignores the interactions between the different generators. The MPC controller designed based on this model may lead to an unsatisfied performance, therefore, the system-wide control performance may not be guaranteed. However, centralized MPC applied to power systems, which are large-scale geographically expansive systems, is impractical. Hence, it is useful to develop a decentralized coordinated MPC method to control of DFIG.

This paper discusses the decentralized coordinated

[†] Corresponding Author: School of Automation Engineering, Northeast Dianli University, China. (lxm0121038@163.com)

^{*} Guang Dong Electric Power Research Institute, China / Southern Power Grid International, Co. LTD, China Southern Power Grid, China.

^{**} State Key Laboratory for Alternate Electric Power system with Renewable Energy Source, North China Electric Power University, China.

^{***} Pleass Global Limited, Water bottling Company, Fiji.

Received: February 9, 2014; Accepted: April 11, 2016

control of DFIG for the first time. By combining interaction measurement method and MPC, a decentralized coordinated MPC is proposed to control the rotor-side converter (RSC) of DFIG. The contents of this paper are arranged as follows:

- The mathematical models of DFIG, SG, and grid are recalled in Section 2.
- In Section 3, an adaptive decentralized-coordinated multiple MPC (ADM-MPC) is proposed, where an artificial neural network trained online is introduced to calculate the weightings.
- In Section 4, a simple, generic RPS in MATLAB environment is used to demonstrate the contributions, while the conclusions are drawn finally.

2. Models of the RPS system

DFIG wind turbines use a wound rotor induction generator (IG), where the rotor winding is fed through a back-to-back converter as shown in Fig. 1 [16, 17]. In this paper, a third-order model of IG is represented for a good compromise between simplicity and accuracy [18, 19].

$$\begin{cases} \dot{E}'_d = -R_r/X_{rr}(E'_d + X_m^2 I_{qs}/X_{rr} + X_m V_{qr}/R_r) + SE'_q \\ \dot{E}'_q = -R_r/X_{rr}(E'_q - X_m^2 I_{ds}/X_{rr} - X_m V_{dr}/R_r) - SE'_d \\ \dot{\omega}_r = \omega_0/H(T_e - T_m - F\omega_r) \end{cases} \quad (1)$$

$$\begin{cases} E'_d = V_{ds} - R_s I_{ds} + X I_{qs} \\ E'_q = V_{qs} - R_s I_{qs} - X I_{ds} \end{cases} \quad (2)$$

$$\begin{cases} P_s = V_{ds} I_{ds} + V_{qs} I_{qs} \\ Q_s = V_{ds} I_{qs} - V_{qs} I_{ds} \end{cases} \quad (3)$$

where the subscripts, ‘r’, ‘s’, ‘d’ and ‘q’ refer to stator, rotor, direct axis and the quadrature axis, respectively. E' , V , I , P , Q , X and R denote equivalent transient voltage, voltage, current, output active power, output reactive power, reactance and resistance, respectively. S is the rotor slip, H is inertia time constant of the rotor of the DFIG,

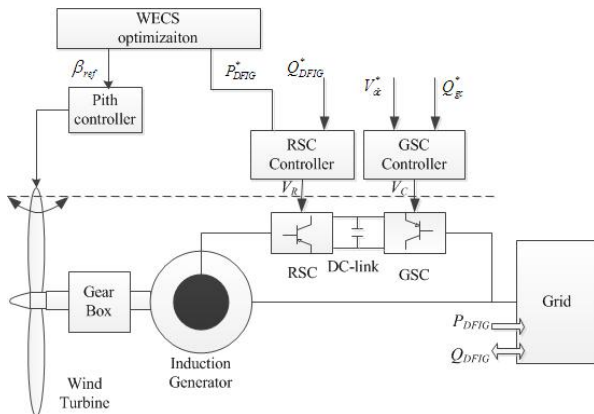


Fig. 1. Schematic representation of a DFIG

F is the damping factor, ω is the angle speed of the rotor of the DFIG, $\omega_0=2\pi f_n$ is the synchronous angle speed. $T_e=E'_d I_{ds} + E'_q I_{qs}$ and T_m are the electromagnetic and mechanical torques, respectively. X_m is the mutual reactance, X' is the equivalent transient reactance of DFIG, $X_{rr}=X_r + X_m$, $X'=X_s + X_m X_r/X_{rr}$.

The standard model of synchronous generator (SG) is [20].

$$\begin{cases} \dot{\delta}_G = \omega_G - \omega_0 \\ \dot{\omega}_G = \omega_0/H_G [P_{Gm} - P_{Ge} - D(\omega_G/\omega_0 - 1)] \\ T'_{d0} \dot{E}'_{Gq} = E_{fd} - E'_{Gq} \end{cases} \quad (4)$$

$$\begin{cases} V_d = X_q I_q \\ V_q = E'_{Gg} - X'_d I_d \end{cases} \quad (5)$$

$$\begin{cases} P_{Ge} = [E'_{Gq} + (X_q - X'_d) I_d] I_q \\ Q_{Ge} = X_q I_q - (E'_{Gq} - X'_d I_d) I_d \end{cases} \quad (6)$$

where the subscript G denotes the variable of SG, D is fraction factor, E_{fd} is the corresponding exciter output voltage, T'_{d0} is the d axis open circuit transient time constant.

In the X - Y synchronous reference frame, the voltage, current and impedance of the i -th node can be written as: $V_{Ti}=V_{Xi}+jV_{Yi}$, $I_{Ti}=I_{Xi}+jI_{Yi}$, $Z_{ij}=R_{ij}+jX_{ij}$, then the networks model with only generator nodes can be written as following form.

$$\begin{bmatrix} V_{X1} \\ V_{Y1} \\ \vdots \\ V_{XN_1} \\ V_{YN_1} \\ \vdots \\ V_{XN} \\ V_{YN} \end{bmatrix} = \begin{bmatrix} R_{11} & -X_{11} & \cdots & R_{1N_1} & -X_{1N_1} & \cdots & R_{1N} & -X_{1N} \\ X_{11} & R_{11} & \cdots & X_{1N_1} & R_{1N_1} & \cdots & X_{1N} & R_{1N} \\ \vdots & \vdots & \vdots & \vdots & \vdots & \vdots & \vdots & \vdots \\ R_{N_1N_1} & -X_{N_1N_1} & \cdots & R_{N_1N_1} & -X_{N_1N_1} & \cdots & R_{N_1N} & -X_{N_1N} \\ X_{N_1N_1} & R_{N_1N_1} & \cdots & X_{N_1N_1} & R_{N_1N_1} & \cdots & X_{N_1N} & R_{N_1N} \\ \vdots & \vdots & \vdots & \vdots & \vdots & \vdots & \vdots & \vdots \\ R_{N1} & -X_{N1} & \cdots & R_{N1} & -X_{N1} & \cdots & R_{NN} & -X_{NN} \\ X_{N1} & R_{N1} & \cdots & X_{N1} & R_{N1} & \cdots & X_{NN} & R_{NN} \end{bmatrix} \begin{bmatrix} I_{X1} \\ I_{Y1} \\ \vdots \\ I_{XN_1} \\ I_{YN_1} \\ \vdots \\ I_{XN} \\ I_{YN} \end{bmatrix} \quad (7)$$

where N_1 is the amount of DFIG nodes, N is the amount of generator nodes, V_{Xi} , V_{Yi} , I_{Xi} and I_{Yi} are the voltages and currents of the X and Y components, respectively. R_{ij} and X_{ij} are the mutual resistance and reactance between the i -th and j -th nodes.

Eq. (7) can be rewritten by using vector-matrix notation.

$$V_F = Z_F I_F \quad (8)$$

3. ADM-MPC Design Method

Small signal modeling method is widely used in the dynamic studies of power systems, such as power system

modeling, eigenvalue analysis and optimal excitation control of SG [20-23]. It has been shown that small signal model of DFIG presents a good accuracy in comparison with the dynamic model [24, 25].

3.1 Interaction measurement model of DFIG

By linearizing Eq. (1)-(6), it can be found that the small signal models of IG and SG have the general form given in Eq. (9)-(10).

$$\begin{cases} \dot{X}_i = A_{1ii}X_i + A_{2ii}\Delta I_{Ti} + B_{ii}U_i + dt_i \\ Y_i = C_{1ii}X_i + C_{2ii}\Delta I_{Ti} \end{cases} \quad (9)$$

$$\Delta E'_i = \Delta V_{Ti} + Z_{dq} \Delta I_{Ti}, \quad (i = 1, 2, \dots, N) \quad (10)$$

where the prefix Δ denotes a small deviation, the details about Eq. (9)-(10) are given in the Appendix A. According to Eq. (8), the small signal model of network is written as

$$\Delta V_F = Z_F \Delta I_F \quad (11)$$

From Eq. (9)-(10), the state space equation for the RPS with N generators can be written as the following form.

$$\begin{cases} \dot{X} = A_1 X + A_2 \Delta I_T + B U + dt \\ Y = C_1 X + C_2 \Delta I_T \end{cases} \quad (12)$$

$$\Delta E' = \Delta V_T + Z_{dq} \Delta I_T \quad (13)$$

where $X, Y, \Delta V, \Delta I_T, \Delta E', dt$ are column vectors and the i -th element of those vectors is corresponding to the variable of the i -th generator. The A_1, A_2, B, C_1, C_2 , and Z_{dq} are block diagonal matrixes and the i -th diagonal block of these is corresponding to the equation of the i -th generator. The linearized forms of terminal voltage and current between the d - q and X - Y frames are

$$\begin{cases} \Delta V_F = \bar{T} \Delta V_T - \bar{T} V_{D0} \Delta \delta \\ \Delta I_F = \bar{T} \Delta I_T - \bar{T} I_{D0} \Delta \delta \end{cases} \quad (14)$$

where δ_i is the angle between q_i axis and X axis.

$$\Delta \delta = \left[\underbrace{0, \dots, 0}_{N_1}, \delta_{N_1+1}, \dots, \delta_N \right]^T, T_{0i} = \begin{bmatrix} \cos \delta_{0i} & \sin \delta_{0i} \\ \sin \delta_{0i} & -\cos \delta_{0i} \end{bmatrix}$$

$$V_{D0} = \text{blockdiag} \left\{ \begin{bmatrix} 0 \\ 0 \end{bmatrix}_{N_1}, \dots, \begin{bmatrix} 0 \\ 0 \end{bmatrix}_{N_1}, \begin{bmatrix} -V_{d0(N_1+1)} \\ V_{q0(N_1+1)} \end{bmatrix}, \dots, \begin{bmatrix} -V_{d0N} \\ V_{q0N} \end{bmatrix} \right\}$$

$$I_{D0} = \text{blockdiag} \left\{ \begin{bmatrix} 0 \\ 0 \end{bmatrix}_{N_1}, \dots, \begin{bmatrix} 0 \\ 0 \end{bmatrix}_{N_1}, \begin{bmatrix} -I_{d0(N_1+1)} \\ I_{q0(N_1+1)} \end{bmatrix}, \dots, \begin{bmatrix} -I_{d0N} \\ I_{q0N} \end{bmatrix} \right\}$$

$$\bar{T} = \text{block} \{ T_1, \dots, T_{N_1}, T_{(N_1+1)0}, \dots, T_{N0} \},$$

Substituting Eq. (14) into Eq. (11),

$$\Delta V_T = Z_t \Delta I_T + K_Z \Delta \delta \quad (15)$$

where $Z_t = \bar{T} Z_F \bar{T}$ and $K_Z = V_{D0} - Z_t I_{D0}$. Eq. (15) is the network equation, which is described by the voltages and currents of stator and rotor angles of generators.

Substituting Eq. (15) into Eq. (13)

$$\Delta I_T = M_1 \Delta E' + M_2 \Delta \delta \quad (16)$$

where $M_1 = (Z_t + Z_{x_{dq}})^{-1}$, $M_2 = -(Z_t + Z_{x_{dq}})^{-1} K_Z$. Obviously,

$$\begin{cases} \Delta E' = M_3 X \\ \Delta \delta = M_4 X \end{cases} \quad (17)$$

Substituting (17) into (16),

$$\Delta I_T = (M_1 M_3 + M_2 M_4) X = M X \quad (18)$$

For avoiding centralized control, Eq. (18) can be rewritten as following form:

$$\begin{bmatrix} \Delta I_{T1} \\ \Delta I_{T2} \\ \vdots \\ \Delta I_{TN} \end{bmatrix} = \begin{bmatrix} M_{11} & M_{12} & \dots & M_{1N} \\ M_{21} & M_{22} & \dots & M_{2N} \\ \vdots & \vdots & \ddots & \vdots \\ M_{N1} & M_{N2} & \dots & M_{NN} \end{bmatrix} \begin{bmatrix} X_1 \\ X_2 \\ \vdots \\ X_N \end{bmatrix} \quad (19)$$

Expanding Eq. (19),

$$\Delta I_{Ti} = M_{ii} X_i + \sum_{\substack{k=1 \\ k \neq i}}^N M_{ik} X_k, \quad (i = 1, 2, \dots, N) \quad (20)$$

Substituting Eq. (20) into Eq. (9),

$$\begin{cases} \dot{X}_i = A_{1ii} X_i + A_{2ii} M_{ii} X_i + A_{2ii} \sum_{\substack{k=1 \\ k \neq i}}^N M_{ik} X_k + B_i U_i + d_{ii} \\ Y_i = C_{1ii} X_i + C_{2ii} M_{ii} X_i + C_{2ii} \sum_{\substack{k=1 \\ k \neq i}}^N M_{ik} X_k \end{cases} \quad (21)$$

Then, the interaction measurement model is obtained as the following.

$$\begin{cases} \dot{X}_i = A_{ii} X_i + B_i U_i + h_{xi} + d_{ii}, \quad (i = 1, 2, \dots, N) \\ Y_i = C_{ii} X_i + h_{yi} \end{cases} \quad (22)$$

$$\begin{cases} h_{xi} = A_{2ii} \sum_{\substack{k=1 \\ k \neq i}}^N M_{ik} X_k = A_{2ii} (\Delta I_{Ti} - M_{ii} X_i) \\ h_{yi} = C_{2ii} \sum_{\substack{k=1 \\ k \neq i}}^N M_{ik} X_k = C_{2ii} (\Delta I_{Ti} - M_{ii} X_i) \end{cases} \quad (23)$$

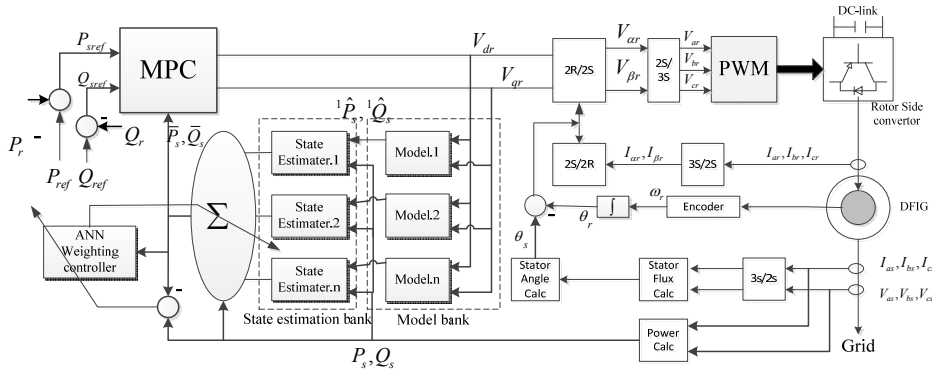


Fig. 2. Control schematic of RSC using ADM-MPC

where $A_{ii}=A_{1ii}+A_{2ii}M_{ii}$, and $C_{ii}=C_{1ii}+C_{2ii}M_{ii}$. The h_{xi} and h_{yi} represent coupled relationship between the i -th generator and the grid. From Eq. (23), it can be seen that those variables only depend on the local signals. This allows that global feedback control to be obtained by only using local signals.

3.2 ADM-MPC controller design

The proposed control schematic is shown in Fig. 2. The trajectory of output active power of stator is $P_{sref}=P_{ref}-P_r$, where P_r is output active power of rotor, and P_{ref} generated by the WECS is the set point of output active power of DFIG. The trajectory of output reactive power of stator Q_{sref} is determined by the operating fashion of DFIG, such as voltage regulator fashion and constant power factor fashion.

3.2.1 Model bank

The full operating range of DFIG can be divided into n operating sub-ranges with n linear models, which adequately represents the local system dynamics within each sub-range. The multiple MPC is based on the discrete state space equation, the discretization of the i -th DFIG model displayed in (22) is

$$\begin{cases} j\hat{X}_{i,k+1} = jF_{ii} j\hat{X}_{i,k} + jG_i U_{i,k} + j\hat{h}_{xi,k} + B_d j d_{ii,k} \\ j\hat{Y}_{i,k+1} = jH_{ii} j\hat{X}_{i,k+1} + j\hat{h}_{yi,k+1} \end{cases} \quad (24)$$

3.2.2 State estimation bank

No model describes the DFIG perfectly everytime for the DFIG characteristics change with time. Thus, a Kalman filter is used to update state vector. In order to cope with the disturbances from wind turbine caused by the various wind speeds, the model in Eq. (24) is updated with the appended state.

The state space equation of wind turbine is

$$\begin{cases} \hat{X}_{di,k+1} = F_{di} \hat{X}_{di,k} + G_{di} n_{di,k} \\ \hat{d}_{di,k+1} = H_{di} \hat{X}_{di,k+1} \end{cases} \quad (25)$$

Combining $j\hat{X}_i$ and $j\hat{X}_{di,k}$, the augment state vector $j\hat{X}_i^a$ is defined as $j\hat{X}_i^a = [j\hat{X}_{i,k} \ j\hat{X}_{di,k}]^T$. This allows for the estimated equation in Eq. (25) to be rewritten with the augment state vector $j\hat{X}_i^a$ as the following form.

$$\begin{cases} \begin{bmatrix} j\hat{X}_{i,k+1} \\ j\hat{X}_{di,k+1} \end{bmatrix} = \begin{bmatrix} jF_{ii,k} & B_{di} jH_{di} \\ 0 & F_{di} \end{bmatrix} \begin{bmatrix} j\hat{X}_{i,k} \\ j\hat{d}_{i,k} \end{bmatrix} + \begin{bmatrix} jG_i \\ 0 \end{bmatrix} U_{i,k} \\ \quad + \begin{bmatrix} jG_{di} \\ 0 \end{bmatrix} j\hat{n}_{di,k} + \begin{bmatrix} j\hat{h}_{xi,k} \\ 0 \end{bmatrix} \\ j\hat{Y}_{i,k+1} = \begin{bmatrix} jH_{ii} & 0 \end{bmatrix} \begin{bmatrix} j\hat{X}_{i,k+1} \\ j\hat{d}_{i,k+1} \end{bmatrix} + j\hat{h}_{yi,k+1} \end{cases} \quad (26)$$

The compact form of Eq. (26) can be written as

$$\begin{cases} j\hat{X}_{i,k+1}^a = jF_i^a j\hat{X}_{i,k}^a + jG_i^a U_{i,k} + jG_{di}^a n_{di,k} + j\hat{h}_{xi,k}^a \\ j\hat{Y}_{i,k+1} = jH_i^a j\hat{X}_{i,k+1}^a + j\hat{h}_{yi,k+1} \end{cases} \quad (27)$$

By using a Kalman filter to update the augment state vector $j\hat{X}_i^a$, the pair of predictor/corrector equations are written as.

$$\begin{cases} j\hat{X}_{i,k|k-1}^a = jF_i^a j\hat{X}_{i,k-1|k-1}^a + jG_i^a U_{i,k-1} + jG_{di}^a n_{di,k-1} j\hat{h}_{xi,k-1}^a \\ j\hat{X}_{i,k|k}^a = j\hat{X}_{i,k|k-1}^a + jL(y_k - jH_i^a j\hat{X}_{i,k|k-1}^a) \\ j\hat{Y}_{i,k|k} = jH_i^a j\hat{X}_{i,k|k}^a + j\hat{h}_{yi,k|k} \end{cases} \quad (28)$$

where y is the output of DFIG, jL denotes Kalman gain of the j -th model in the model bank, which can be solved from the steady-state Ricatti equation independently of the other model's Kalman gains [26].

3.2.3 Model predictive control

Assuming that jw_i is the weightness of the j -th model of the i -th generator, the output of average linear model of DFIG can be defined as

$$\bar{y}_{i,k+p|k} = \sum_{j=1}^n w_{i,k}^j \hat{y}_{i,k+p|k}^j \quad (29)$$

where $\hat{y}_{i,k+p|k}^j$ ($P=1,2,\dots, N_{pi}$) terms are the individual model predicted outputs and calculated as described in Eq. (27) and Eq. (28), N_{pi} is the predictive horizon. From the average linear model output described in Eq. (29), the performance of the i -th DFIG can be written as the following form.

$$\min J_i = (R_i - \bar{Y}_i)^T W_{yi} (R_i - \bar{Y}_i) + \Delta U_i^T W_{ui} \Delta U_i \quad (30)$$

where $R_i = [P_{sre} \ Q_{sreff}]^T$ is the vector of set points, \bar{Y}_i is the vector of predicted outputs from $\bar{y}_{i,k+1|k}$ to $\bar{y}_{i,k+N_p|k}$, and ΔU_i is the optimal control movement. The optimization problem can be solved analytically for ΔU_i , the proof is given in Appendix B

$$\Delta U_i = \left(Se_i^T Sc_i^T W_{yi} Sc_i Se_i + W_{ui} \right)^{-1} Se_i^T Sc_i^T W_{yi} (R - Sx_i - Sc_i U_{oi}) - G_i \quad (31)$$

where,

$$G_i = \left(Se_i^T Sc_i^T W_{yi} Sc_i Se_i + W_{ui} \right)^{-1} Se_i^T Sc_i^T W_{yi} (S_{hxi} + S_{di} + S_{hyi}).$$

3.2.4 Model weighting calculation

To cope with the nonlinearity and continuous variation of operating points of DFIG, a back propagation (BP) ANN is employed as a weighting controller to improve the approximation performance. The mathematic description of the BP ANN is shown as the following form.

$$\begin{cases} net_m^H(k) = \sum_{j=1}^M w_{mj}^H x_j, O_m^H(k) = f[net_m^H(k)] \\ net_l^O(k) = \sum_{j=1}^Q w_{lj}^O O_m^H, O_l^O(k) = g[net_l^O(k)] \\ m = 1, 2, \dots, Q \quad l = 1, 2, \dots, n \end{cases} \quad (32)$$

where net^H , net^O , O^H and O^O are the input and output of the hidden and output layers, respectively. w^H and w^O are the weights of hidden and output layers, respectively. M , Q and n are the numbers of input, hidden, and output layers respectively. $f[\bullet]$ and $g[\bullet]$ are activation functions.

Thus, the l -th output of the BP ANN is the weighting of the l -th model in the model bank. In the following derivation, the subscript ' i ' denoted the i -th generator is neglected to avoid confusion for that there are a few subscripts used in the ANN description.

$${}^1w(k) = O_1^O(k), {}^2w(k) = O_2^O(k), \dots, {}^n w(k) = O_n^O(k) \quad (33)$$

The performance of the ANN is defined as

$$E(k) = \frac{1}{2} [y(k) - \bar{y}(k)]^2 \quad (34)$$

where y_i is the output of DFIG, and \bar{y}_i is the output of the average model described by Eq. (29). By using gradient descent method, the w_{im}^O can be updated online as the following form.

$$\Delta w_{im}^O(k) = -\eta \frac{\partial E(k)}{w_{im}^O} + \alpha \Delta w_{im}^O(k-1) \quad (35)$$

where η is a learning rate and α is a momentum factor.

$$\frac{\partial E(k)}{w_{im}^O} = \frac{\partial E(k)}{\partial \bar{y}(k)} \frac{\partial \bar{y}(k)}{\partial \Delta u} \frac{\partial \Delta u}{\partial O_l^O(k)} \frac{\partial O_l^O(k)}{\partial w_{im}^O} \quad (36)$$

The $\partial O_l^O(k) / \partial w_{im}^O$ can be obtained easily by using BP method with Eq. (32). The $\partial \bar{y}(k) / \partial \Delta u$ is the Jacobian matrix of DFIG, which can be calculated by using its sign [27] and the $\partial \Delta u / \partial O_l^O(k)$ can be calculated by using Eq. (31). It's not difficult to solve. By using a similar approach, the w_{mj}^H can be obtained conveniently. The weightings can be obtained by using Eq. (32). Based on the above derivations, it is noted that the ANN based weighting controller is a nonlinear closed-loop control, which takes the natural advantage of DFIG and provides a better approximation performance than linear weighting methods.

From Eq. (31), it can be seen that the obtained control law of AMD-MPC is only related to local signals. The G_i can be regarded as the impact of coordinated signals on the final control law, and the weightings of the average model of DFIG can be updated online according to the output error. Hence, the proposed AMD-MPC can be considered as an adaptive decentralized coordinated control, which is a desirable feature of control for DFIG.

It should be pointed out that this method can be conveniently extended to control of SG as the SG and DFIG have the generic model by using the interaction measurement modeling method.

4. Dominant Eigenvalue Analysis and Simulation

The configuration and power flow of RPS are shown in Fig. 3, which is composed of two subsystems, the thermal power and the wind power subsystems. The parameters of RPS, included DFIG, transmission lines, transformers, SGs, excitation systems and governors are given in Appendix A. Simulations are performed in comparison with the proposed ADM-MPC, Bayesian probability based decentralized coordinated multiple MPC (BDM-MPC), and rotor-side conventional PI controller. The BDM-MPC has the same control structure with ADM-MPC, however the

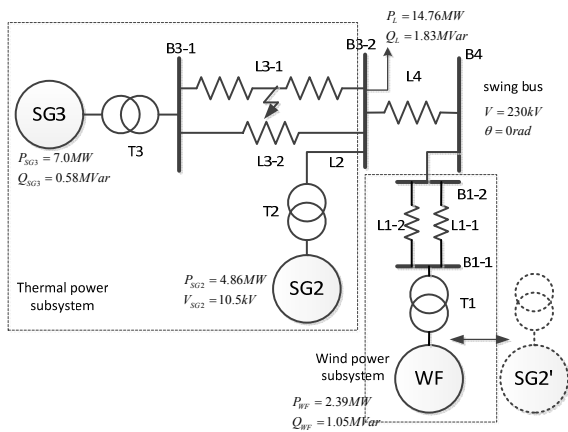


Fig. 3. Configuration of RPS

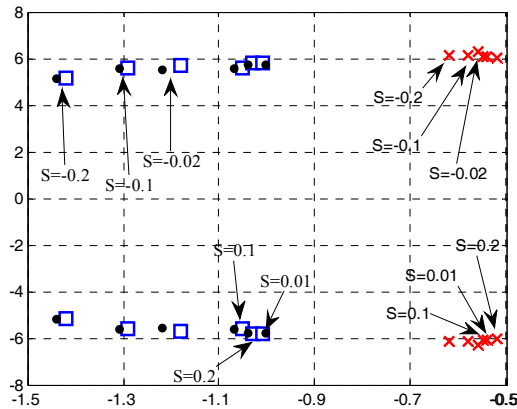


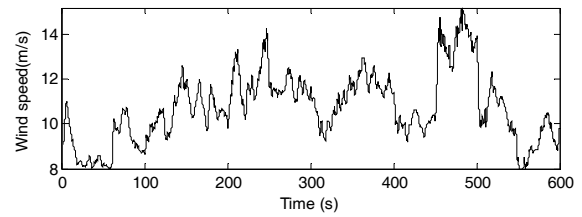
Fig. 4. Influence of RSC control loop on the dominant eigenvalue over operating slip range (With PI controller \times ; with BDM-MPC controller \square , with ADM-MPC controller \bullet .)

weighting of BDM-MPC is calculated by using a Bayesian probability based method [28].

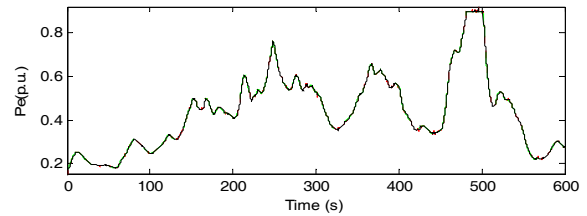
4.1. Dominate eigenvalue analysis

The locations of dominant eigenvalue pairs with PI, BDM-MPC and ADM-MPC controllers for various values of slip over the permitted operating range are displayed in Fig. 4, where $\{S\} = \{0.2, 0.1, 0.01, -0.1, -0.2\}$ are chosen to establish the model bank of DFIG.

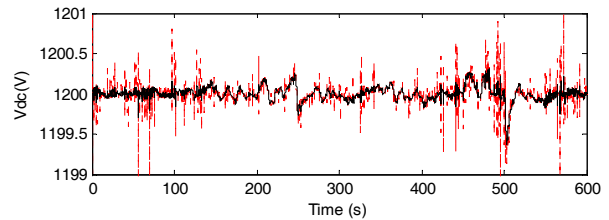
When rotor-side PI controller is installed into DFIG, the eigenvalues cluster in a group having real parts mainly in the range -0.5 to -0.6. This corresponds to damping factors of approximately 0.08 to 0.10. When the ADM-MPC is introduced, the eigenvalues are shifted considerably to the left in the complex plane, indicating that the damping of the dominant oscillation is significantly influenced. At a slip value of $S=0.2$, the real part of the dominant eigenvalue is -1.04, corresponding to damping factor is 0.1783. For a value of $S=-0.2$ (the highest rotor speed), corresponding to the highest active power level, the real part has a value of -



(a) Effective wind speed



(b) Output of active power



(c) DC-link voltage

Fig. 5. MPPT control performance under effective wind speed over the full operating region of DFIG: ADM-MPC (full line), BDM-MPC (dotted line), Set points (dashed line)

1.44, corresponding to a damping factor of 0.2698, which is approximately 270% higher than the PI controller used. It was noted that the damping of the RPS system with ADM-MPC controller was significantly enhanced over the full operating region of DFIG.

It can also be seen that DFIG with the BDM-MPC and ADM-MPC controllers has approximate locations of dominant eigenvalues in the operating points chosen for modeling. At value of $S=-0.02$ excluded from the modeling points, the damping factors with those two decentralized-coordinated controllers are 0.2154 and 0.2020 respectively, the difference between them is very little.

4.2. Simulation of MPPT control

In order to verify the maximum power point tracking (MPPT) performance of DFIG with the proposed ADM-MPC, simulation was performed under the effective wind speed [29], and the results were shown in Fig. 5, where P_e and V_{dc} denote the output of active power (in per unit) and DC-link voltage of DFIG, respectively. From Fig. 5, it is seen that both ADM-MPC and BDM-MPC provide an accurate tracking performance over the full operating region of DFIG. In order to directly understand the difference of MPPT performance between those two controllers, a few sample values of output active power are

Table 1. Sample values of active power with different controllers

Time	100s	200s	300s	400s	500s	600s
Set Points	0.2484	0.4134	0.5304	0.5501	0.8981	0.2769
ADMMPCC	0.2485	0.4136	0.5305	0.5500	0.8980	0.2767
BDMMPCC	0.2462	0.4120	0.5300	0.5505	0.8980	0.2771

shown in Table 1.

From Table 1, it can be seen that the errors of MPPT with ADM-MPC is less than 0.02% p.u., which is smaller than BDM-MPC used. This means DFIG with ADM-MPC can provide a better MPPT performance in comparison with BDM-MPC used

$$\dot{V}_{dc} = (P_c - P_r) / CV_{dc} \quad (37)$$

The model of DC-link displays in Eq. (37), where $C=0.01F$, P_c and P_r denote the DC-link capacitor, the active power of the grid-side converter (GSC) and the active power of rotor-side converter, respectively. According to Eq. (37), a dynamic balance between P_c and P_r can reduce the fluctuation of DC-link voltage. For the adaptive online weighting algorithm of the ADM-MPC, a better fitting performance is achieved. This reduces active power accumulated in the DC-link, therefore the fluctuation of V_{dc} with ADM-MPC is smoother. The evidence is shown in Fig. 5(c).

4.3. Simulations under three-phase ground fault

In order to study the transient stability of DFIG with the proposed ADM-MPC controller, three-phase ground faults with the different ground resistance were applied at the wind power subsystem and the thermal power subsystem, respectively. For that the dynamics of the IG are much faster than the turbine dynamics, the wind speed can be regarded as a constant in the transient study by using small signal modeling method [22].

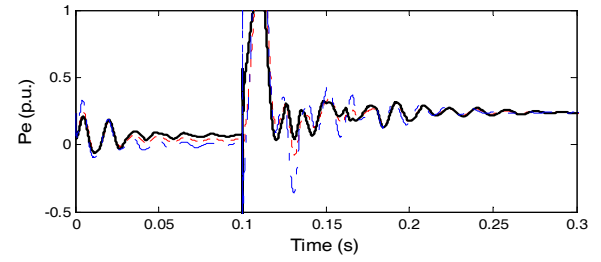
Case 1: Three-phase ground faults with ground resistance decreasing step by step were applied in the middle of the transmission lines L3-1 and L1-1at $t=0^+$ s respectively, and the faults were cleared after 0.1s. The results were shown in Fig. 6 and Fig. 7.

In the transient control of DFIG, it is known that the sudden change of transient electromotive force vector (E'_d and E'_q) from its steady value should be confined in an acceptable range for reducing drop of terminal voltage [30]., With (A-4), the objective of MPC controller is rewritten as the following form where the wind speed is considered as a constant in the transient control.

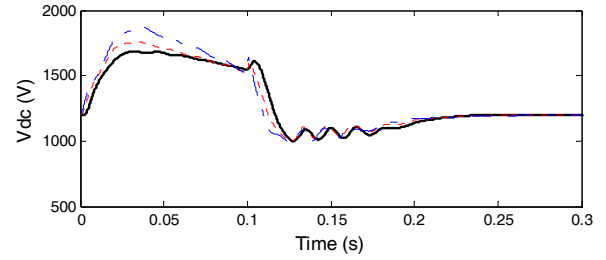
$$J_i = (-\bar{Y}_i)^T W_{yi} (-\bar{Y}_i) + \Delta U_i^T W_{ui} \Delta U_i \quad (38)$$

$$= Sx_i^T W_{yi}^* Sx_i + \Delta U_i^T W_{ui}^* \Delta U_i + P$$

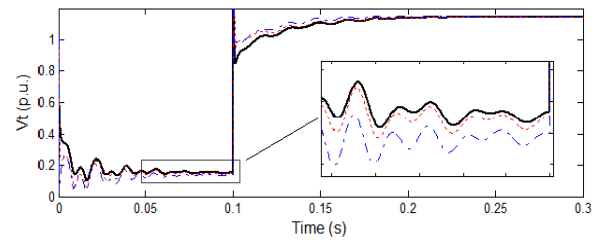
$$P = (S_c U_{i0} + S_{hxi} + S_{di} + S_{hyi})^T W^* (S_c U_{i0} + S_{hxi} + S_{di} + S_{hyi})$$



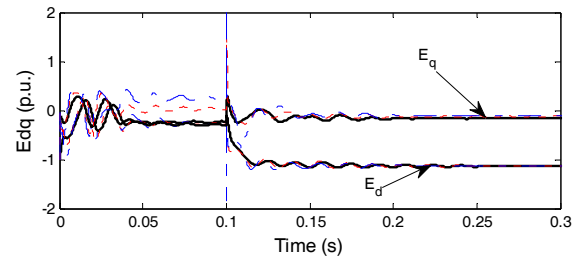
(a) Output of active power



(b) DC-link voltage



(c) Terminal voltage



(d) Vector of E_d and E_q

Fig. 6. Response of three-phase ground fault applied at line L3-1: $S=0.1$, ADM-MPC (full line), BDM-MPC (dotted line), PI controller (dashed dotted line)

Form Eq. (38), it is seen that the objective can be transferred into a state regulator in the transient control. This means the variation of state variable $X_i = [\Delta\omega, \Delta E'_{qi}, \Delta E'_{di}]^T$ will be minimized to smaller than its steady state before the fault.

From Fig. 6(d) and Fig. 7(d), it can be seen that the oscillation of transient electromotive force vector with AMD-MPC is smaller in comparison with the others two controllers used. This is the reason why the drop of terminal voltage of DFIG with AMD-MPC is lower. A lower drop of terminal voltage was contributed to improve the fault ride-through (FRT) capability of DFIG. Therefore

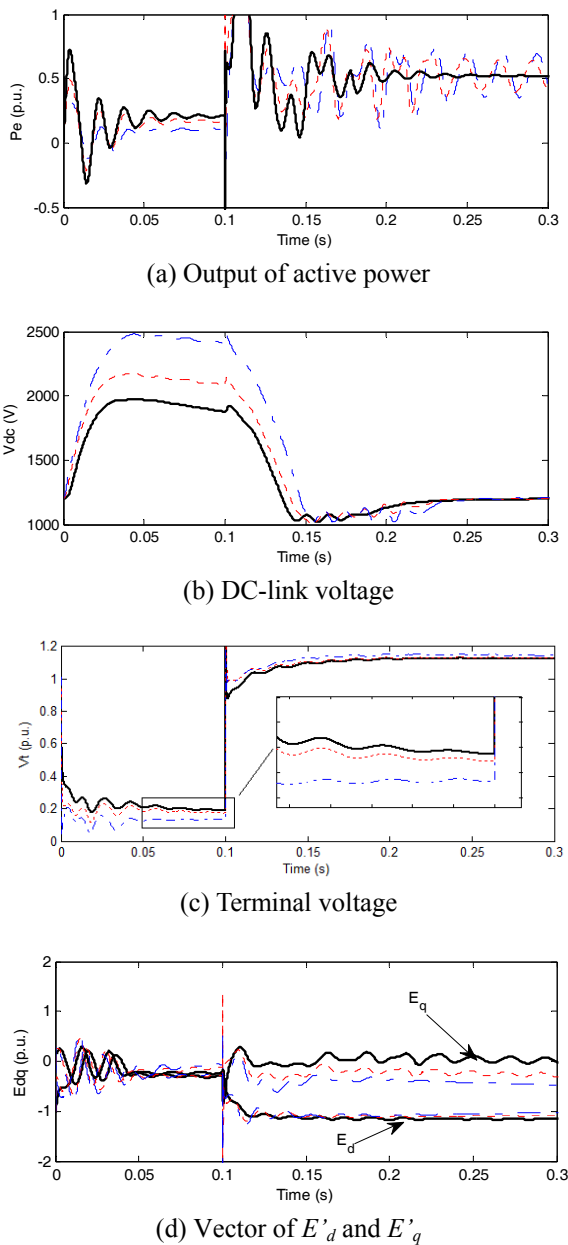


Fig. 7. Response of three-phase ground fault applied at line L1-1: $S=-0.02$, ADM-MPC (full line), BDM-MPC (dotted line), PI controller (dashed dotted line)

the DFIG was able to be connected with the grid and generate more active power. Thus, less active power was accumulated in the capacitor, and the DC-link voltage was lower, which also contributed to the improvement of FRT. The evidences are shown in Fig. 6(a)-(c) and Fig. 7(a)-(c). Fig. 6 also confirms the dominant eigenvalue analysis shown in Fig. 4.

According Fig. 4, it was noted that DFIG with AMD-MPC and BDM-MPC had almost the same damping contribution at $S=-0.02$. However, Fig. 7(a) demonstrates that DFIG with AMD-MPC has a better damping performance than BDM-MPC used. It is known that dominant eigenvalue analyses are based on the steady state.

During or after the fault, the parameters and structure of power system can be changed dramatically. However, this transient characteristic is shown inadequately by dominant eigenvalue analysis. Moreover, BMD-MPC is based on a linear weightiness method, which cannot provide a satisfied fitting performance for the system with strong nonlinearity. However, AMD-MPC has an ANN based nonlinear weighting controller, which can be adjusted online according to the objective function. This gives AMD-MPC an adaptive capability during the fault, which can explain the conflict between dominant eigenvalue analysis and time response simulation.

Fig. 6 and Fig. 7 demonstrate that decentralized coordinated MPC provides DFIG with capability of damping contribution over the full operating region included both sub-synchronous and super-synchronous points.

It is noted here that the protection system of DFIG has not been considered in the simulations for clearly seeing the detailed and complete responses during the faults. Actually, DFIG will be tripped by the protection system as soon as DC-link voltage exceeding 1900V.

Case 2: For showing the characteristics of excitation systems of SG and DFIG, the WF in the RPS is replaced by a SG, which has the same parameters with SG2. The replaced system is called conventional power system (CPS).

A three phase to ground fault was applied at bus B3-1 of CPS and RPS at $t=0^+$, respectively. The critical clearing times (CCT) of those two systems were calculated under different controllers such as conventional PI controller, BDM-MPC controller and the proposed ADM-MPC controller.

It is known that both automatic voltage regulator (AVR) and power system stabilizer (PSS) of SG manipulate the magnitude of rotor flux vector, since the position of the rotor flux is dictated by the physical position of the rotor itself. Hence, there must be a compromise between the designs excitation control system of AVR and PSS. In contrast, a DFIG has the capability of manipulating both the magnitude and the position of the rotor flux vector and as a consequence of this possesses a much greater control capability than a SG. The evidence of capabilities of DFIG and SG in the excitation control system was shown in Table 2 and Table 3.

From Table 2, it can be seen that CCTs of CPS with decentralized coordinated MPC controller installed is

Table 2. CCTs of the CPS with different controllers

	AVR+PSS	BDM-MPC	ADM-MPC
CCT (s)	0.6103	0.6502	0.6525
Increase of CCT	0%	6.54%	6.91%

Table 3. CCTs of the RPS with different controllers

	PI	BDM-MPC	ADM-MPC
CCT (s)	0.6432	0.6651	0.6684
Increase of CCT	5.39%	8.98%	9.52%

higher than AVR and PSS. When DFIG based WF was installed in RPS, PI controller installed in the DFIG, the CCT of RPS is 0.6432s, which is close to the maximum value of CCT of CPS with decentralized coordinated MPC controller. The CCTs of RPS with ADM-MPC and BDM-MPC are higher than that of CPS with the same controllers. These confirms the above analysis of the excitation system of SG and DFIG. From Table 2 and Table 3, it can be concluded that the transient stability is improved by using this type of decentralized-coordinated MPC controllers.

It is noted that the parameters of AVR and PSS of SG are tuned based on the original value of Simpower system and simulation conditions to guarantee the reasonability of results comparisons between the different controllers.

5. Conclusions

In this paper, an ADM-MPC design method was proposed that can significantly enhance the tracking performance and transient stability of DFIG. The proposed ADM-MPC had shown to provide a DFIG-based WF with consistently enhanced contribution to grid damping over the full operating region of DFIG. By the eigenvalues analysis, it is demonstrated that the dominant eigenvalues are shifted considerably to the left of the complex plane, which indicates that the damping of the RPS system is considerably enhanced.

This paper demonstrated that a suitable control of a DFIG not only improved the efficiency of wind power conversion, but also provided WFs with the capability of contributing significantly to network support and operation with respect to system damping and transient stability.

Appendix A

1. For DFIG ($i = 1, 2, \dots, N_1$)

$$A_{1ii} = \begin{bmatrix} -\frac{\omega_0 F}{2H} & \frac{\omega_0 I_{QS0}}{2H} & \frac{\omega_0 I_{DS0}}{2H} \\ E'_{D0} & -\frac{R_R}{X_{RR}} & \omega_{r0} - 1 \\ -E'_{Q0} & 1 - \omega_{r0} & -\frac{R_R}{X_{RR}} \end{bmatrix},$$

$$A_{2ii} = \begin{bmatrix} \frac{\omega_0 E'_{Q0}}{2H} & \frac{\omega_0 E'_{D0}}{2H} \\ 0 & R_R \frac{X_M^2}{X_{RR}} \\ -R_R \frac{X_M^2}{X_{RR}} & 0 \end{bmatrix}, \quad B_{ii} = \begin{bmatrix} 0 & 0 \\ 0 & \frac{X_M}{X_{RR}} \\ -\frac{X_M}{X_{RR}} & 0 \end{bmatrix},$$

$$C_{1ii} = \begin{bmatrix} 0 & I_{QS0} & I_{DS0} \\ 0 & -I_{DS0} & I_{QS0} \end{bmatrix},$$

$$C_{2ii} = \begin{bmatrix} 2R_S I_{QS0} + E'_{Q0} & 2R_S I_{DS0} + E'_{D0} \\ -2X' I_{QS0} + E'_{D0} & -2X' I_{DS0} - E'_{Q0} \end{bmatrix}$$

$$X_i = \begin{bmatrix} \Delta\omega_i \\ \Delta E'_{qi} \\ \Delta E'_{di} \end{bmatrix}, Y_i = \begin{bmatrix} \Delta P_{si} \\ \Delta Q_{si} \end{bmatrix}, U_i = \begin{bmatrix} \Delta V_{qri} \\ \Delta V_{dri} \end{bmatrix}, \Delta I_{Ti} = \begin{bmatrix} \Delta I_{qsi} \\ \Delta I_{dsi} \end{bmatrix},$$

$$\Delta E'_i = \begin{bmatrix} \Delta E'_{qi} \\ \Delta E'_{di} \end{bmatrix}, \Delta V_{Ti} = \begin{bmatrix} \Delta V_{qsi} \\ \Delta V_{dsi} \end{bmatrix}, Z_{dqi} = \begin{bmatrix} -R_{si} & -X'_i \\ X'_i & -R_{si} \end{bmatrix}.$$

$$dt_i = \begin{bmatrix} \Delta T_{mi} & \frac{\omega_{0i}}{H_i} & 0 & 0 \end{bmatrix}^T.$$

The mechanical torque of DFIG is modeled as a measured disturbance here [11].

2. For SG ($i = N_1 + 1, N_1 + 2, \dots, N$)

$$A_{1ii} = \begin{bmatrix} 0 & 0 & 1 \\ 0 & -\frac{1}{T'_{d0j}} & 0 \\ 0 & -\frac{\omega_0}{H_{Gj}} I_{q0j} & -\frac{D_j}{H_{Gj}} \end{bmatrix}, \quad B_{ii} = \begin{bmatrix} 0 \\ \frac{1}{T'_{d0j}} \\ 0 \end{bmatrix}, \quad dt_i = \begin{bmatrix} 0 \\ 0 \\ 0 \end{bmatrix}$$

$$A_{2ii} = \begin{bmatrix} 0 & 0 \\ 0 & \frac{(X_{dj} - X'_{dj})}{T'_{d0j}} \\ -\frac{\omega_0}{H_{Gi}} [E'_{Gq0j} + (X_{qj} - X'_{dj}) I_{d0j}] & -\frac{\omega_0}{H_{Gi}} (X_{qj} - X'_{dj}) I_{q0j} \end{bmatrix},$$

$$C_{1ii} = \begin{bmatrix} 0 & I_{q0} & 0 \\ 0 & -I_{d0} & 0 \end{bmatrix},$$

$$C_{2ii} = \begin{bmatrix} E'_{Gq0} + (X_q - X'_{d0}) I_{d0} & (X_q + X'_{d0}) I_{q0} \\ 2X_q I_{q0} & 2X'_d I_{d0} - E'_{Gq0} \end{bmatrix},$$

$$X_i = \begin{bmatrix} \Delta\delta_{Gi} \\ \Delta E'_{Gqi} \\ \Delta\omega_{Gi} \end{bmatrix}, Y_i = \begin{bmatrix} \Delta P_{Gei} \\ \Delta Q_{Gei} \end{bmatrix}, U_i = \begin{bmatrix} 0 \\ \Delta E'_{fdi} \end{bmatrix}, \Delta I_{Ti} = \begin{bmatrix} \Delta I_{qi} \\ \Delta I_{di} \end{bmatrix},$$

$$\Delta E'_i = \begin{bmatrix} \Delta E'_{Gqi} \\ 0 \end{bmatrix}, \Delta V_{Ti} = \begin{bmatrix} \Delta V_{qi} \\ \Delta V_{di} \end{bmatrix}, Z_{dqi} = \begin{bmatrix} 0 & X'_{di} \\ -X_{qi} & 0 \end{bmatrix}.$$

Comparing to electrical torque of SG, the mechanical torque is a slow time-varying variable. So, it can be regarded as a constant in the small signal modeling of SG [22].

3. Parameters of RPS system

The model and the parameters of rotor-side PI controller of DFIG can found in the Renewable Energy Library of Application Libraries.

The parameters of SGs, exciting system and governor and PSS can be found in the “power_PSS” Demo of SimPowerSystems of MATLAB v2012.a.

Transformers (T1)

V1=230kV, R1=3.674 Ω , L1=0.292H; V2=575V, R2=6.89×10⁻⁵Ω, L2=5.482×10⁻⁶H, Rm=2.204×10⁶Ω, Lm=+∞H

Transformers (T2,T3)

V1=230kV, R1=5.878×10⁻⁵Ω, L1=0.024H,

V2=10.5kV, R2=4.444×10⁻⁷Ω, L2=0H;

Rm=222.22Ω, Lm=0.59H

Transmission Lines:

positive and zero-sequence resistance:

0.053 and 1.61Ω

positive and zero-sequence inductance:

0.0014and 3.32×10⁻³H/km

positive and zero-sequence capacitance:

11.33×10⁻⁹ and 5.01×10⁻⁹C/km

Lengths:

L1-1 and L1-2: 10km; Line L2: 3km;

Line L3-1and L3-2: 50km; Line L4: 20km.

The normal frequency f_n used in the simulations is 60 Hz.

Appendix B

From Eq. (29), the propagation of \bar{Y}_i must be determined, which is started with $\bar{Y}_{i,k+1|k}$. Expanding $\bar{Y}_{i,k+1|k}$

$$\bar{Y}_{i,k+1|k} = \sum_{j=1}^n {}^j w_{i,k} {}^j \hat{y}_{i,k+1|k} = {}^1 w_{i,k} ({}^1 H_i {}^1 \hat{X}_{i,k+1}^a + {}^1 \hat{h}_{yi,k+1}) + \dots + {}^n w_{i,k} ({}^n H_i {}^n \hat{X}_{i,k+1}^a + {}^n \hat{h}_{yi,k+1}) \quad (A1)$$

$$U_{i,k+1} = U_{i,k} + \Delta U_{i,k+1} \quad (A2)$$

Substituting Eq. (27) into Eq. (A1)

$$\begin{aligned} \bar{Y}_{i,k+1|k} = & {}^1 w_{i,k} ({}^1 H_i {}^1 F_i^a {}^1 \hat{X}_{i,k}^a + {}^1 H_i {}^1 G_i^a U_{i,k} \\ & + {}^1 H_i {}^1 \hat{h}_{xi,k} + {}^1 G_{di}^a n_{di} + {}^1 \hat{h}_{yi,k+1}) + \dots, \\ & + {}^n w_{i,k} ({}^n H_i {}^n F_i^a {}^n \hat{X}_{i,k}^a + {}^n H_i {}^n G_i^a U_{i,k} \\ & + {}^n H_i {}^n \hat{h}_{xi,k} + {}^n G_{di}^a n_{di} + {}^n \hat{h}_{yi,k+1}) \end{aligned} \quad (A3)$$

It is important to note here that this process of expansion can be continued in a similar fashion for $\bar{Y}_{i,k+2|k}$ to $\bar{Y}_{i,k+N_p|k}$. Using Eq. (A1)-(A3), along with the equivalents for $\bar{Y}_{i,k+2|k}$ to $\bar{Y}_{i,k+N_p|k}$, \bar{Y}_i can be written as

$$\bar{Y}_i = Sx_i + Sc_i Se_i \Delta U_i + Sc_i U_{i0} + S_{hxi} + S_{di} + S_{hyi} \quad (A4)$$

Where the vectors ΔU_i , U_{i0} , S_{hxi} , S_{di} and S_{hyi} and matrices Sx_i , Sc_i , and Se_i are defined as following.

$$\begin{aligned} \Delta U_i &= [\Delta U_{i,k}, \Delta U_{i,k+1}, \dots, \Delta U_{i,k+N_{ui}-1}]_{1 \times N_{ui}}^T \\ U_{i0} &= [U_{i,k-1}, \dots, U_{i,k-1}]_{1 \times N_{pi}}^T \\ S_{hxi} &= \sum_{j=1}^n {}^j w_{i,k} \begin{bmatrix} {}^j H_i^a & \dots & 0 \\ \vdots & \ddots & \\ {}^j H_i^a & {}^j F_i^{a^{N_p-1}} & \dots & {}^j H_i^a \end{bmatrix}_{N_{pi} \times N_{pi}} \begin{bmatrix} {}^j h_{xi,k}^a \\ \vdots \\ {}^j h_{xi,k+N_p-1}^a \end{bmatrix}_{N_{pi} \times 1} \\ S_{di} &= \sum_{j=1}^n {}^j w_{i,k} \begin{bmatrix} {}^j H_i^a & \dots & 0 \\ \vdots & \ddots & \\ {}^j H_i^a & {}^j F_i^{a^{N_p-1}} & \dots & {}^j H_i^a \end{bmatrix}_{N_{pi} \times N_{pi}} \begin{bmatrix} {}^j G_{di}^a n_{di,k} \\ \vdots \\ {}^j G_{di}^a n_{di,k+N_p-1} \end{bmatrix}_{N_{pi} \times 1} \\ S_{hyi} &= \sum_{j=1}^n {}^j w_{i,k} \begin{bmatrix} {}^j h_{yi,k+1}^a \\ \vdots \\ {}^j h_{yi,k+N_p}^a \end{bmatrix}_{N_{pi} \times 1}, \quad Se_i = \begin{bmatrix} I & 0 \\ \vdots & \ddots \\ I & \dots & I \end{bmatrix}_{N_{pi} \times N_{ui}} \\ Sx_i &= \sum_{j=1}^n {}^j w_{i,k} \begin{bmatrix} {}^j H_i^a & {}^j F_i^a \\ {}^j H_i^a & {}^j F_i^{a^2} \\ \vdots & \vdots \\ {}^j H_i^a & {}^j F_i^{a^{N_p}} \end{bmatrix}_{N_{pi} \times 1} \quad {}^j \hat{X}_{i,k|k}^a \\ Sc_i &= \sum_{j=1}^n {}^j w_{i,k} \begin{bmatrix} {}^j H_i^a & {}^j G_i^a & \dots & 0 \\ \vdots & \ddots & \ddots & \\ {}^j H_i^a & {}^j F_i^{a^{N_p-1}} & {}^j G_i^a & \dots & {}^j H_i^a & {}^j G_i^a \end{bmatrix}_{N_{pi} \times N_{pi}} \end{aligned}$$

Where I denotes an identity matrix, N_{pi} is the predictive horizon, and N_{ui} is the control horizon.

Acknowledgment

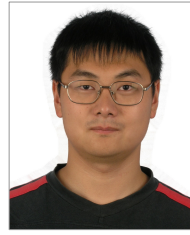
This work is supported by the National Key Basic Research Program of China (973 Program) under grant No. 2012CB215203, by the National Nature Science Foundation of China under grant No. 61203043, by State Key Laboratory of Alternate Electrical Power System with Renewable Energy Sources (Grant No. LAPS14014), and by the Fundamental Research Funds for the Central Universities in China.

References

- [1] Mahdi Hayatdavudi, Mojtaba Saeedimoghadam, Seyed M.H Nabavi, “Adaptive control of pitch angle of wind turbine using a novel strategy for manage-

- ment of mechanical energy generated by turbine in different wind velocities,” *Journal of Electrical Engineering & Technology* vol. 8, pp. 863-871, Jul. 2013.
- [2] J Lee, J Kim, YH Kim, et al, “Rotor speed-based droop of a wind generator in a wind power plant for the virtual inertial control,” *Journal of Electrical Engineering & Technology* vol. 8, pp. 1021-1028, Sep. 2013.
- [3] Lyu, Jae-Kun, et al, “Impacts of wind power integration on generation dispatch in power systems,” *Journal of Electrical Engineering & Technology*, vol. 8, pp. 453-463, May 2013.
- [4] El-Moursi M. S, Bak-Jensen B, Abdel-Rahman M. H., et al, “Novel STATCOM controller for migrating SSR and damping power system oscillations in a series compensated wind park,” *IEEE Trans. Power Electr*, vol. 25, pp. 429-421, Aug. 2010.
- [5] Yang L., Yang G. Y., Xu Z., et al, “Optimal controller design of a doubly-fed induction generator wind turbine system for small signal stability enhancement”, *IET Gener. Transm. Distrib.*, vol. 4, pp. 579-597, May 2010.
- [6] M.Y. amamoto, O. Motoyoushi, “Active and reactive control of doubly fed wound rotor induction generator”, *IEEE Trans. Power Electron*, vol. 6, pp. 624-629, Oct. 1991.
- [7] R. Pena, J. C. Clare, G. M. Asher, “Doubly fed induction generator using back to back PWM converters and its application to variable-speed wind-energy generation,” *Pron. Inst. Elect. Power*, vol. 143, pp. 231-241, May 1996.
- [8] F. M. Hughes, O. Anaya-lara, N. Jenkin, et al, “Control of DFIG-based wind generation for power network support,” *IEEE Trans. Power Syst.*, vol. 20, pp. 1958-1966, Nov. 2005.
- [9] J. B. Ekanayake, L. Holdsworth, X. G. Hu, et al., “Dynamic modeling of doubly fed induction generator wind turbine,” *IEEE Trans. Power Syst.*, vol. 18, pp. 803-809, May 2003
- [10] Zhang Xin-fang, Xu Da-ping, Liu Yi-bing, “Predictive functional control of a doubly fed induction generator for variable speed wind turbines,” *Fifth World Congress on Intelligent Control and Automation*, 2004, pp. 3315-3319.
- [11] Kaneko A., Sakai, Hara N. et al, “Model predictive control of DFIG-based wind turbines,” *American Control Conference*, 2012, pp. 2264-2269.
- [12] Guolian Hou, Zhentao Wang, Pan Jiang, “Multi-variable predictive functional control applied to doubly fed induction generator under unbalanced grid voltage conditions,” *4th IEEE Conference on Industrial Electronics and Applications*, 2009, pp. 2644-2650.
- [13] Sguarezi Filho A J, de Oliveira Filho M E, Ruppert E, “A predictive control strategy for doubly-fed induction generator direct power control” *Industry Applications (INDUSCON)*,” 9th IEEE/IAS International Conference on. IEEE, 2010, pp. 1-6.
- [14] Phan V. T., Lee, H. H., “Improved predictive current control for unbalanced stand-alone doubly-fed induction generator-based wind power systems,” *IET Electric Power Applications*, Vol. 5, pp. 275-287, Mar. 2011.
- [15] Soliman M., Malik O. P., Westwick D. T., “Multiple Model Predictive Control for Wind Turbines With Doubly Fed Induction Generators,” *IEEE Transaction on Sustainable Energy*, vol. 2, pp. 215-225, Jul. 2011.
- [16] S. Muller, M. Deicke and Rik W. De Doncker, “Doubly fed induction generator systems for wind turbines,” *IEEE Industry Applications Magazine*, vol. 8, pp. 26-33, May 2002.
- [17] R. Pena, J. C. Clare, G. M. Asher, “Doubly fed induction generator using back-to-back PWM converters and its application to variable-speed wind-energy generation,” *IEEE Proc.-Electr. Power Appl.*, vol. 143, May 1996.
- [18] Andrés Feijóo, José Cidrás, and Camilo Carrillo, “A third order model for doubly fed induction machine”, *Electroc Power systems research*, vol. 56, pp. 121-127, Nov. 2000.
- [19] J. B. Ekanayake, L. Holdsworth, and N. Jenkin, “Comparison of 5th order and 3rd order machine models for doubly fed induction generator (DFIG) with turbines,” *Elect Power Syst. Res.*, vol. 67, pp. 2207-2215, Dec. 2003.
- [20] P. Kundu, “Power system stability and control,” EPRI New York: McGraw-Hill, 1994.
- [21] M. Huang, H. J. Chen, Y. D. Han, Z. H. Wang, “Multimachine power system stabilizer based on decentralized optimal control theory,” *IFAC multi-machine power systems modeling and control applications*, Brussels, 1988.
- [22] Y. D. Han, Z. H. Wang, and H. J. Chen, “Optimal decentralized coordinated control of power systems,” *BeiJing: Tsinghua University Press*, 1996.
- [23] Singh. M. G, “Decentralized control,” *New York: Elsevier Science Inc.*, 1981.
- [24] Jose Cidras, and Andres Eltas Feijoo, “A linear dynamic model for asynchronous wind turbines with mechanical fluctuations,” *IEEE Trans. Power Syst.*, vol. 17, pp. 681-687, Aug. 2002.
- [25] F.Wu, X.P. Zhang, K. Godfrey, and P. Ju, “Small signal stability analysis and optimal control of a wind turbine with doubly fed induction generator,” *Proc. Inst. Elect. Eng., Gen., Transm, Distrib*, vol. 1, pp. 751-760, Sep. 2007.
- [26] Lewis F., “Optimal Estimation,” *New York: John Wiley & Sons, Inc*, 1986.
- [27] Saerens M, Soquet A., “Neural controller based on back-propagation algorithm,” *IEE Proceedings F (Radar and Signal Processing)*, 1991, pp. 55-62.

- [28] M. Kuure-Kinsey, and B. W. Bequette, "Multiple model predictive control: A state estimation based approach," In Proc. Amer. Control Conf., 2007, pp. 3739-3744.
- [29] H. Camblong, M. R. Vidal, and J. R. Puiggali, "Principles of a simulation model for a variable-speed pitch-regulated wind turbine," Wind Eng., vol. 28, pp. 157-175, Jul. 2004.
- [30] Anaya Lara O, Hughes F M, Jenkins N, et al., "Rotor flux magnitude and angle control strategy for doubly fed induction generators," Wind energy, vol. 9, pp. 479-495, Sep. 2006



power markets.

Ming-yang LI He received Eng. D. degree from Tsinghua University. He is currently with the State Key Laboratory of Alternate Electrical Power System with Renewable Energy Sources. His research interests include modeling and optimization of complex networked systems, power system operations and



Noel Vishal Nathan He received Eng. B. degree from North China Electric Power University in 2015. He is now an electrical and plant engineer in Pless Global Limited, Water bottling Company in Fiji.



Xiao-ming LI He received Eng. D. degree in control theory and engineering from North China Electric Power University. He is currently an associate professor in Northeast Dianli University. His research interest is renewable power system modeling and control.



Xi ZHANG Dr. ZHANG is Senior Engineer in Guangdong Electric Power Research Institute. He is mainly engaged in the research on advanced process control and optimization of thermal power plant.



control.

Zhong-wei LIN He received Eng. D. degree from Beijing University of Aeronautics and Astronautics in 2011. He is now an associate professor in North China Electric Power University. His research interests include stochastic control, nonlinear control, renewable energy power system modeling and



Yu-guang NIU He received Eng. D. degree from North China Electric Power University in 1997. He is now Professor and Doctoral Supervisor of control theory and engineering in the School of Control and Computer Engineering at North China Electric Power University.